



Deposited via The University of Leeds.

White Rose Research Online URL for this paper:

<https://eprints.whiterose.ac.uk/id/eprint/157180/>

Version: Accepted Version

---

**Article:**

Sardar, S, Kale, G and Ghadiri, M (2020) Influence of processing conditions on the ionic conductivity of holmium zirconate (Ho<sub>2</sub>Zr<sub>2</sub>O<sub>7</sub>). *Ceramics International*, 46 (8 Part B). pp. 11508-11514. ISSN: 0272-8842

<https://doi.org/10.1016/j.ceramint.2020.01.177>

---

© 2020 Elsevier Ltd and Techna Group S.r.l. All rights reserved. This manuscript version is made available under the CC-BY-NC-ND 4.0 license <http://creativecommons.org/licenses/by-nc-nd/4.0/>.

**Reuse**

This article is distributed under the terms of the Creative Commons Attribution-NonCommercial-NoDerivs (CC BY-NC-ND) licence. This licence only allows you to download this work and share it with others as long as you credit the authors, but you can't change the article in any way or use it commercially. More information and the full terms of the licence here: <https://creativecommons.org/licenses/>

**Takedown**

If you consider content in White Rose Research Online to be in breach of UK law, please notify us by emailing [eprints@whiterose.ac.uk](mailto:eprints@whiterose.ac.uk) including the URL of the record and the reason for the withdrawal request.

# Influence of Processing Conditions on the Ionic Conductivity of Holmium Zirconate ( $\text{Ho}_2\text{Zr}_2\text{O}_7$ )

Suneela Sardar, Girish Kale<sup>\*</sup>, Mojtaba Ghadiri

School of Chemical and Process Engineering, University of Leeds, Leeds LS2 9JT, U.K.

\*Corresponding Author: [g.m.kale@leeds.ac.uk](mailto:g.m.kale@leeds.ac.uk)

## Abstract

Nanopowders of holmium zirconate ( $\text{Ho}_2\text{Zr}_2\text{O}_7$ ) synthesised through carbon neutral sol-gel method were pressed into pellets and individually sintered for 2h in a single step sintering (SSS) process from 1100°C to 1500°C at 100°C interval and in a two step sintering (TSS) process at (I) -1500°C for 5min followed by (II) - 1300°C for 96h. Relative density of each of the sintered pellet was determined using the Archimedes' technique and the theoretical density was calculated from crystal structure data. Grain size was obtained from SEM micrographs using ImageJ. Pellets processed by TSS have been found to be denser (98%) with less grain growth (1.29 $\mu\text{m}$ ) as compared to the pellets processed using SSS process. Ionic conductivity of  $\text{Ho}_2\text{Zr}_2\text{O}_7$  pellets sintered by two different processes was measured using ac impedance spectroscopy technique over the temperature range of 350°C to 750°C in the frequency range of 100 mHz to 100 MHz for both heating and cooling cycles. The temperature dependence of bulk ( $2.67 \times 10^{-3} \text{ S.cm}^{-1}$ ) and grain boundary ( $2.50 \times 10^{-3} \text{ S.cm}^{-1}$ ) conductivities of  $\text{Ho}_2\text{Zr}_2\text{O}_7$  prepared by TSS process are greater than those processed by SSS process suggesting the strong influence of processing conditions and grain size. Results of this study, indicates that the TSS is the preferable route for processing the holmium zirconate as it can be sintered to exceptionally high densities at lower temperature, exhibits less grain growth and enhanced ionic conductivity compared with the samples processed by SSS process. Hence, holmium zirconate can be considered as a promising new oxide ion conducting solid electrolyte for intermediate temperature SOFC applications between 350°C to 750°C temperature range.

**Keywords:** *Sintering, densification, two step sintering, impedance spectroscopy, ionic conductivity, activation energy, holmium zirconate*

## Introduction

Lanthanide based binary oxides crystallising in pyrochlore structure have received significant attention in recent years due to their diverse applications. Their properties such as semi-conducting behaviour <sup>[1]</sup>, ionic conductivity <sup>[2, 3]</sup>, ferromagnetism <sup>[4]</sup>, luminescence <sup>[5, 6]</sup>,

radiation stability <sup>[7, 8]</sup> have been explored in their respective fields of applications. Oxide pyrochlores found their applications as antireflective/protective coatings and refractory matrices for optical devices, dielectric ceramics for microwave wireless communication devices, nuclear waste-storage materials, catalysts and oxygen conductors in fuel cells <sup>[9]</sup>. Oxide pyrochlores have been recently considered as potential materials for applications as solid electrolytes <sup>[10]</sup> in the intermediate temperature solid oxide fuel cells (IT-SOFC).

$A_2B_2O_7$  type lanthanide zirconates occur as one of two closely related isometric structures at ambient conditions, such as pyrochlore and disordered fluorite-type structure. Relative structural stability between pyrochlore and fluorite can be predicted by the tolerance factor which is related to the ionic radius ratio of cations in A and B sites ( $r_A/r_B$ ). For lanthanide pyrochlores the disordered phase forms at equilibrium when  $r_A/r_B < 1.46$  <sup>[11]</sup>. The disordered structure is similar to the mineral fluorite ( $CaF_2$ ), with a single cation and anion site <sup>[12]</sup>. Pyrochlore zirconates with defect fluorite structure possess important potential applications such as catalyst and oxygen ion conductors in fuel cells <sup>[13]</sup>.

$Ho_2Zr_2O_7$  previously prepared by Polymerized-Complex Method (PCM) <sup>[14]</sup> and gel combustion technique followed by high temperature sintering <sup>[15]</sup>. These methods involve milling and high temperature processing to obtain nanopowders.

Leeds Alginate Process (LAP) is an environmental friendly carbon neutral sol-gel technique developed and researched by Kale and co-workers <sup>[16, 17]</sup> for the formation of single phase multicomponent oxide nanoparticles of functional ceramics at temperature below 600°C. This process is known to yield reproducibly and consistently a pure single phase materials <sup>[16, 17]</sup> and good control over homogeneity and stoichiometry of multicomponent metal oxide nanoparticles <sup>[18]</sup>. As part of larger research programme, we have recently synthesised for the first time holmium zirconate ( $Ho_2Zr_2O_7$ ) nanoparticles having cubic defect-fluorite structure below 600°C through LAP and reported its thermal, decomposition and crystal structure properties <sup>[19]</sup>.

In this research article we report for the first time our results of optimisation of the densification of nanopowder compacts of  $Ho_2Zr_2O_7$  by single step sintering (SSS) and two step sintering (TSS) processes, determination of microstructure and the grain growth in sintered compacts between 1100°C to 1500°C and, investigate the influence of processing and microstructure on the bulk and grain boundary conductivity of sintered  $Ho_2Zr_2O_7$  compacts using ac impedance spectroscopy over a range of temperature between 350°C to 750°C.

## Experimental Section

Nanopowders of holmium zirconate prepared using LAP described in our earlier work <sup>[19]</sup> were pressed into twenty five pellets of 13mm diameter and 1.5mm thickness at 5kN load in a steel die using a uniaxial press. First, fifteen pellets were sintered in ambient atmosphere using a single step sintering (SSS) process over the temperature range of 1100°C to 1500°C at an interval of 100°C for 2h at each temperature with the heating and cooling rate of 3 °C/min. The remaining pellets were sintered using a two step sintering (TSS) process in which pellets were heated at 3°C /min to 1500°C for 5min in first step and then cooled to 1300°C, corresponding to 75% of theoretical density and held at that temperature for further 96h in the second step to achieve further densification without further grain growth. Different temperatures and time intervals were studied for TSS process to find out the conditions to achieve maximum relative density and minimum grain growth.

Bulk density measurement of Ho<sub>2</sub>Zr<sub>2</sub>O<sub>7</sub> pellets sintered by SSS and TSS was measured using the Archimedes' principle and relative density was calculated with the help of theoretical density obtained from the powder X-ray crystallography data.

Microstructure of holmium zirconate pellets sintered by two different processes were examined by scanning electron microscopy (SEM) using a Hitachi SU8230 and grain growth was analysed using ImageJ software. Sintered pellets were ground, polished finely using standard metallography techniques and thermally etched before performing SEM analysis. Pellets were ground to remove the top layer and then polished with 3µm diamond paste to achieve the smooth surface finish. Thermal etching of all the sintered and polished pellets was carried out by heating individual pellet for 1 hr at the temperature 50°C below their respective sintering temperature i.e. if sintering is at 1300°C then thermal etching is at 1250°C.

Samples for ac impedance spectroscopy were prepared by carefully coating, opposite faces of each of the sintered pellet with conductive silver paste and fired at 800°C for 1h to remove any binder present in it to metallise the contact surfaces in order to minimise interfacial impedance between the sample surface and platinum measuring leads. The frequency range of 100 mHz to 100 MHz with an excitation voltage of 10 mV, using a Solartron SI1260 impedance analyser, was employed for the impedance measurements as a function of temperature between 350°C to 750°C. During the impedance measurements the pellets were spring loaded in a bespoke quartz rig to provide firm contact between the sample surface and measuring leads. The quartz rig was housed in the Faraday cage within a horizontal tube furnace in order to prevent electric

field from the furnace wire windings affecting impedance measurements. The impedance analyser was controlled using Z-plot whereas the data was analysed using Z-view (Scribner Associates) and plotted in Origin Pro software.

## **Results and Discussion**

### **Density and Microstructure**

Pellets of holmium zirconate ( $\text{Ho}_2\text{Zr}_2\text{O}_7$ ) were sintered using single step sintering (SSS) and two step sintering (TSS) processes. The variation of percentage relative density and percentage residual porosity of the sintered pellets as a function of sintering temperature using SSS and TSS is shown in Fig. 1. It can be clearly seen in Fig. 1 that the relative density of  $\text{Ho}_2\text{Zr}_2\text{O}_7$  pellets sintered using SSS process is increasing systematically and correspondingly the porosity is decreasing with increase in sintering temperature. The relative density of samples sintered at  $1500^\circ\text{C}$  using SSS process was found to be  $92 (\pm 0.4)\%$  and corresponding porosity decrease to  $8 (\pm 0.6) \%$ . Furthermore, the relative density appears to be stabilising at around  $92\%$  as seen in Fig. 1 in a SSS process.

In a TSS process, the sample is first heated to a temperature corresponding to highest relative density as obtained by the SSS process to attain an intermediate density for short time and then held at lower temperature corresponding to  $75\%$  of the theoretical density for a prolonged duration <sup>[20]</sup>. In this investigation samples are heated in the first step to  $1500^\circ\text{C}$  for 5min to achieve the intermediate density and in the subsequent step the samples are held at  $1300^\circ\text{C}$ , corresponding to greater than  $75\%$  theoretical density for 96h to achieve maximum density. It can be seen in Fig. 1 that the samples held for 72h in the second step were only  $83\%$  dense. It should be noted that for the second step of TSS process the temperature chosen is  $1300^\circ\text{C}$  as the relative density achieved at this temperature during SSS process is greater than  $75\%$ . At this temperature the pores in the sample became subcritical and unstable against shrinkage <sup>[20, 21]</sup> hence, as seen in Fig. 1 the relative density achieved in this study is  $98 (\pm 0.3)\%$  for  $\text{Ho}_2\text{Zr}_2\text{O}_7$  by TSS process compared with the  $92\%$  achieved by SSS process.

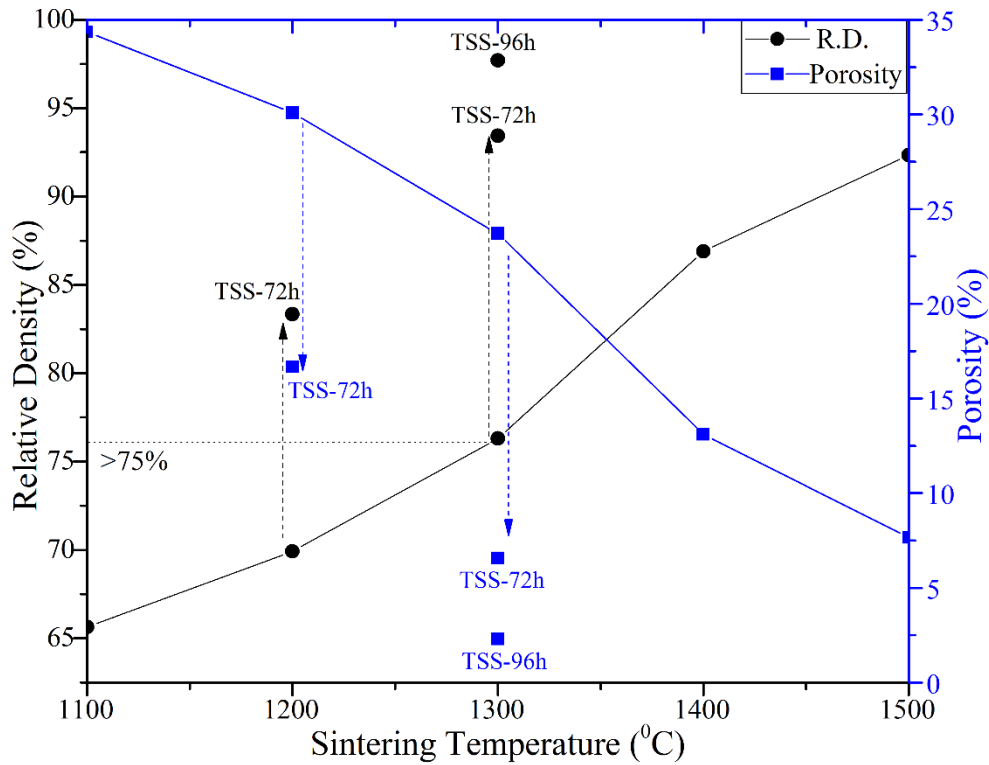


**Fig. 1: Effect of sintering temperature on the relative density and porosity of holmium zirconate pellets. Two step sintering (TSS): (I) - 1500°C for 5min, (II) - 1300°C for 96h.**

Micrographs from (a) to (e) in Fig. 2 represent those of the samples sintered using SSS process and (f) is for the one using TSS process. Thermal etching of all the polished pellets reveal the clear grain boundary in SEM micrographs. The grain size was calculated from the SEM micrographs of the thermally etched polished sample using ImageJ. The average grain size was measured from three different micrographs using ImageJ at each temperature and the pictures shown in the article are best visual images obtained with clear grain boundary and clean surface. The growth in the grain size has increased with the increase in sintering temperature from (a) to (e) along with the densification in case of single step sintering (SSS) even the scale is same for all the micrographs. TSS processed sample (f) shows less grain growth as compared to the SSS processed samples at higher temperatures; 1400°C and 1500°C.

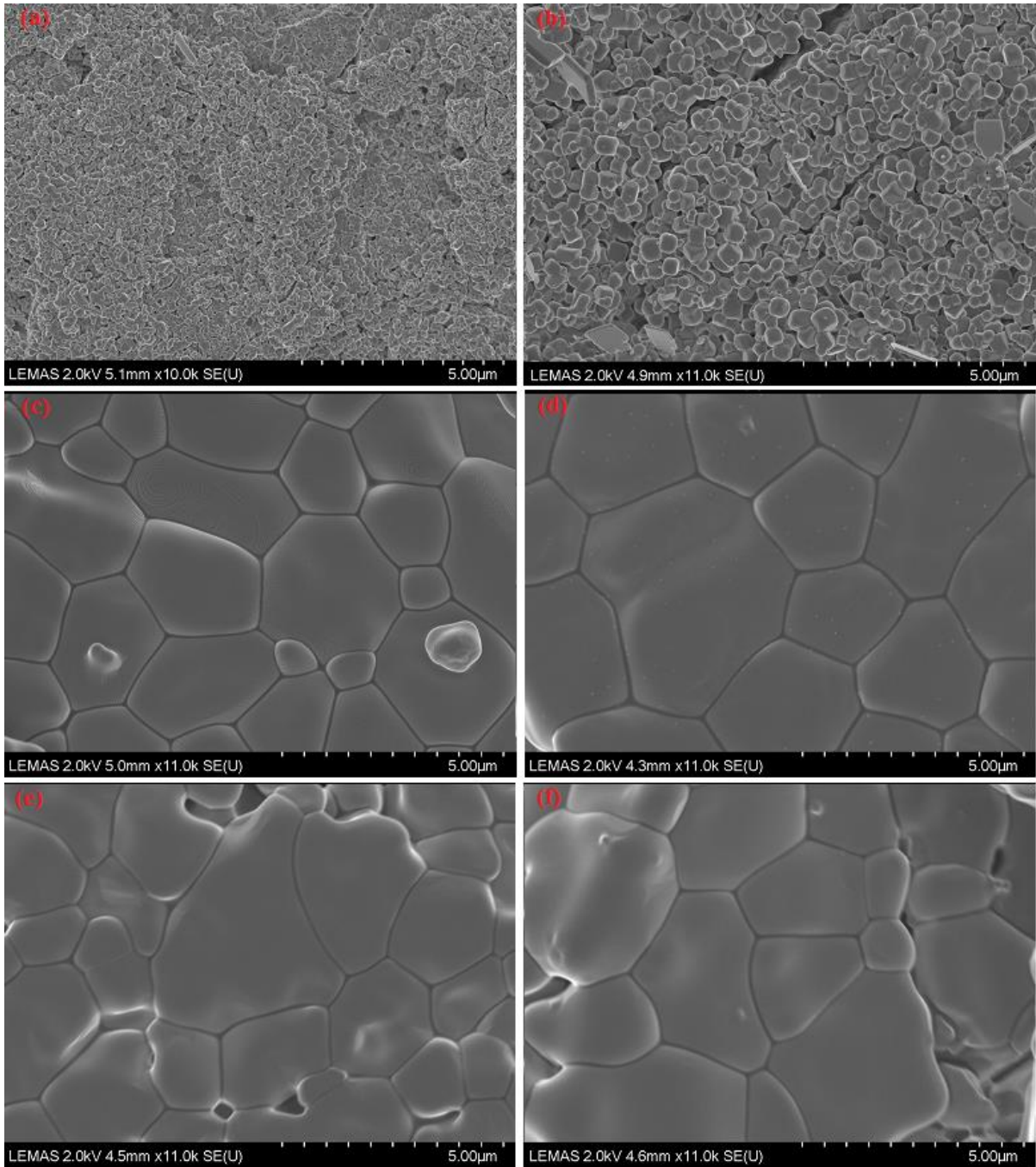


**Fig. 2: SEM micrographs of sintered  $\text{Ho}_2\text{Zr}_2\text{O}_7$  pellets. From (a) to (e) are the micrographs of the pellets after single step sintering (SSS) for 2h at (a) 1100°C (b) 1200°C (c) 1300°C (d) 1400°C (e) 1500°C and (f) after two step sintering (TSS): (I) - 1500°C for 5min, (II) - 1300°C for 96h.**

The variation of grain size of thermally etched pellet samples of  $\text{Ho}_2\text{Zr}_2\text{O}_7$  as a function of the relative density of the samples sintered using SSS and TSS process respectively is shown in Fig. 3. It can be seen in Fig. 3 that with the increase in relative density there is increase in grain size for samples sintered from 1100°C to 1500°C using the SSS process. Furthermore, Fig. 3 shows that as the sintering temperature approaches 1300°C the relative density and grain size

increases sharply suggesting that this is the critical temperature for the sudden enhancement in mass transfer rate in  $\text{Ho}_2\text{Zr}_2\text{O}_7$  which leads to enhanced grain growth. However, interestingly for samples sintered using the TSS process at  $1300^\circ\text{C}$ , the grain size remains almost unchanged at about  $1.29 (\pm 0.1)\mu\text{m}$  whereas the relative density reaches a maximum of 98%, nearly 6% greater than the samples sintered using SSS process at  $1500^\circ\text{C}$ . The variation in density of  $\text{Ho}_2\text{Zr}_2\text{O}_7$  samples sintered using SSS and TSS process is in good agreement with the microstructure of samples shown in Fig. 2. Hence, the TSS process is a favourable approach to achieve greater densification of nanopowder ceramic samples and suppressing the grain growth as second sintering step proceeds with a frozen microstructure and has slower diffusion kinetics that is sufficient to achieve maximum density [20].

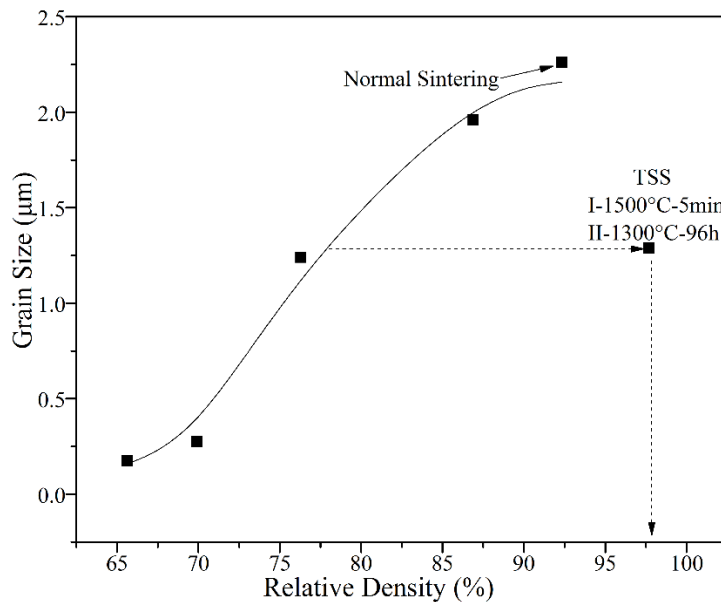


**Fig. 3: Variation of grain size and relative density as a function of sintering temperature of  $\text{Ho}_2\text{Zr}_2\text{O}_7$  pellet samples. Sintering temperature increases with  $100^\circ\text{C}$  interval from left to right starting from  $1100^\circ\text{C}$  to  $1500^\circ\text{C}$ .**

Smaller grain size of oxide with higher density is likely to enhance the fracture toughness and improve the tolerance limit of solid electrolytes against thermal shock in SOFC [21]. Similar results were obtained in the earlier investigation of cerium gadolinium oxide (CGO) by Wang et al [22].

### Ac Impedance Spectroscopy

Typical Nyquist plots of  $\text{Ho}_2\text{Zr}_2\text{O}_7$  sintered at  $1500^\circ\text{C}$  for 2h using SSS process measured at  $350^\circ\text{C}$  and  $550^\circ\text{C}$  are shown in Fig. 4 for both heating and cooling cycles. At  $350^\circ\text{C}$  only a single semicircle response was recorded which corresponds to the bulk contribution as shown

in Fig. 4(a) suggesting that grain boundary contribution is negligible. On the contrary two semicircles were recorded at 550°C as shown in Fig. 4(b) which correspond to the bulk contribution at higher frequency and grain boundary effects at lower frequency. The radius of semicircles decreases with the increase in temperature indicating the presence of thermally activated bulk conduction process [23]. The results of heating and cooling cycles have been found to be almost identical throughout the temperature range of measurement from 350°C to 750°C akin to those shown in Fig. 4(a and b) at 350°C and 550°C. This indicates that the  $\text{Ho}_2\text{Zr}_2\text{O}_7$  solid electrolyte respond reversibly in the temperature range of measurement, which is an important behaviour of solid electrolytes as they are subject to temperature variation when used in an electrochemical device [24].

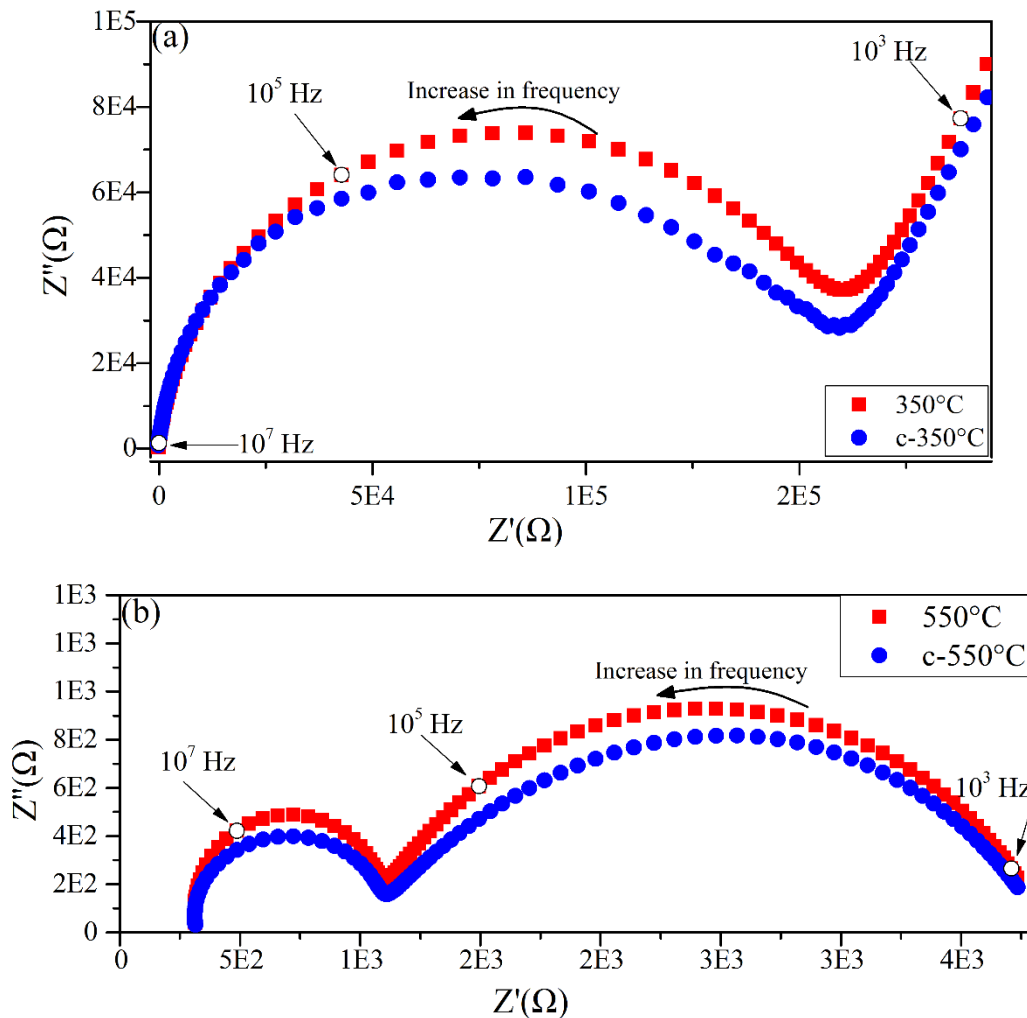


**Fig. 4:** Complex impedance plots for  $\text{Ho}_2\text{Zr}_2\text{O}_7$  sintered at 1500°C for 2h measured in heating cycle at (a) 350°C and (b) 550°C, (c-350°C and c-550°C for cooling cycle).

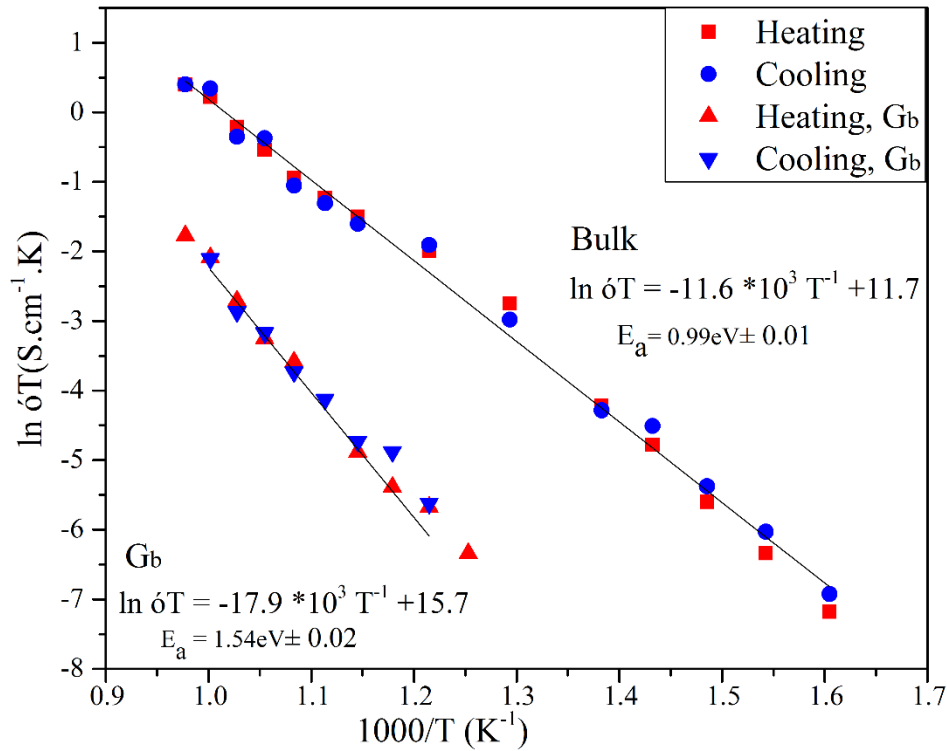
The temperature dependence of the electrical conductivity ( $\sigma_T$ ) was analysed using an Arrhenius expression of the form

$$\sigma_T = \sigma_0 \exp(-Ea/kT) \quad (1)$$

where  $\sigma_0$  is pre-exponential factor related to the effective number of mobile charge carriers,  $T$  is the absolute temperature,  $k$  is Boltzmann constant and  $Ea$  is the activation energy for oxide ion migration. The value of activation energy for ionic conduction in  $\text{Ho}_2\text{Zr}_2\text{O}_7$  has been obtained by plotting  $\ln\sigma_T$  against  $1/T$  as shown in Fig. 5 for bulk and grain boundary of single step sintered  $\text{Ho}_2\text{Zr}_2\text{O}_7$  pellet measured over the temperature range of 350°C to 750°C and frequency range of 100 mHz to 100 MHz for both heating and cooling cycles.

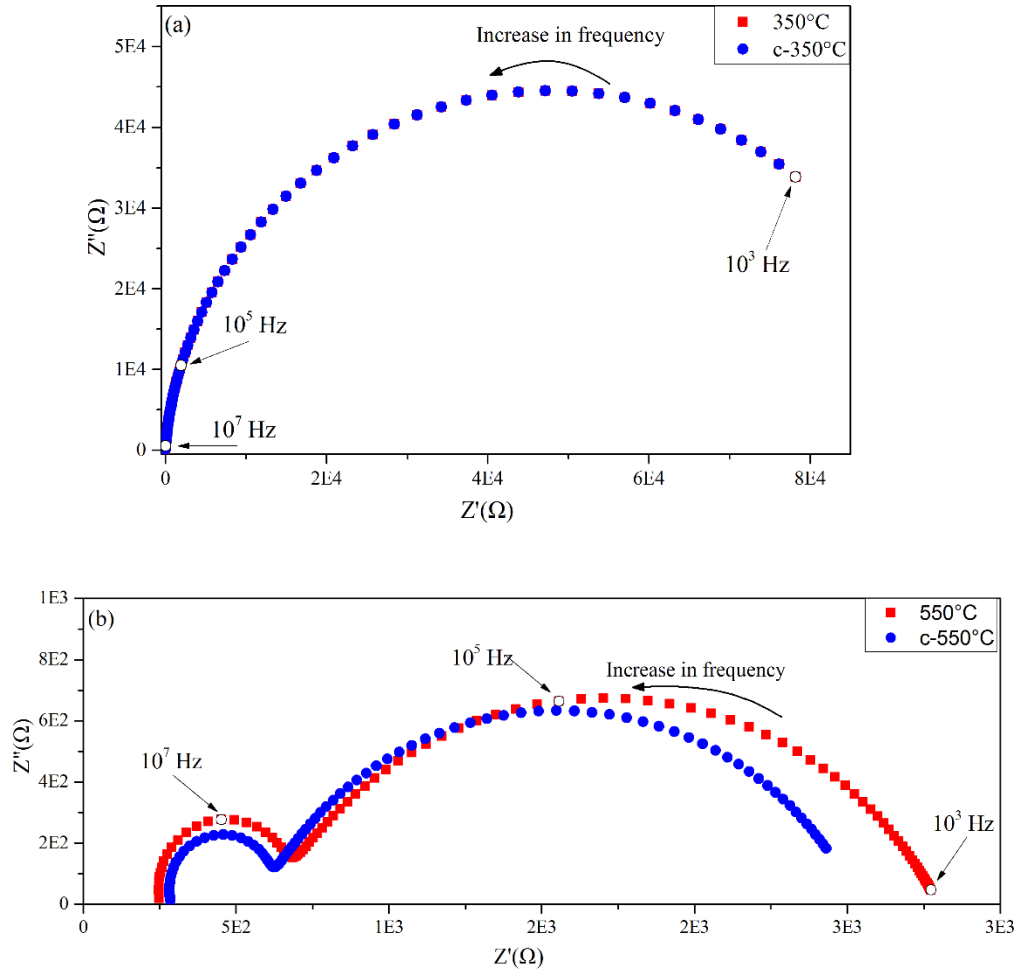
The ionic conductivity of  $\text{Ho}_2\text{Zr}_2\text{O}_7$  has been found to increase with increase in temperature following the Arrhenius behaviour thereby confirming that ionic diffusion in the material is thermally activated. The average value of activation energy for bulk ionic conduction has been found to be 0.99 ( $\pm 0.01$ ) eV by combining data for both heating and cooling cycles. This value is comparable with activation energy (0.9 eV) of ionic conductivity of CGO pellets prepared by SSS<sup>[22]</sup> process. The magnitude of activation energy for ionic conduction of  $\text{Ho}_2\text{Zr}_2\text{O}_7$  has been found to be slightly lower than that for the conventional solid electrolytes Ytria Stabilized Zirconia-YSZ (1.01 eV) and comparable with Gadolinium Doped Ceria (GDC) (0.9 eV)<sup>[25]</sup>.

Fig. 5 compares the Arrhenius plot of grain boundary conductivity for both heating and cooling cycles with that of the bulk. The effect of grain boundary started appearing at temperature greater than 527°C. The combined average value of activation energy for grain boundary conductivity for both heating and cooling cycles has been found to be 1.54 ( $\pm 0.02$ ) eV. The grain boundary conductivity in samples prepared by SSS process has been  $1.66 \times 10^{-4} \text{ S.cm}^{-1}$  which is lower than that of bulk  $1.46 \times 10^{-3} \text{ S.cm}^{-1}$  at 750°C as shown in Table 1. Lower grain boundary conductivity over the entire temperature range reflecting the defective nature of grain boundary compared with the bulk of grains.



**Fig. 5: Temperature dependence Arrhenius plots of bulk and grain boundary conductivity in heating and cooling cycles of holmium zirconate pellets sintered at 1500°C for 2h using SSS process.**

Figs. 6 shows the results of the impedance spectroscopy measurements at 350°C and 550°C of holmium zirconate pellets sintered using the two step sintering (TSS) process. Unlike in the samples prepared using SSS process complex impedance of bulk  $\text{Ho}_2\text{Zr}_2\text{O}_7$  measured at 350°C and 550°C for both heating and cooling cycles shown in Fig. 6 (a and b) is in good agreement with each other whereas that for the grain boundary component is in reasonable agreement. At 350°C the conductivity of the sample is entirely due to the bulk contribution and there is no sign of grain boundary contribution as shown in Fig. 6(a). With the increase in temperature there appears two semicircles which suggests that there is a noticeable contribution of both bulk and grain boundary towards the conductivity as shown in Fig. 6(b).



**Fig. 6: Complex impedance plots for  $\text{Ho}_2\text{Zr}_2\text{O}_7$  with two step sintering; (I) -  $1500^\circ\text{C}$  for 5min, (II) -  $1300^\circ\text{C}$  for 96h measured in heating cycle at (a)  $350^\circ\text{C}$  and (b)  $550^\circ\text{C}$ , (c- $350^\circ\text{C}$  and c- $550^\circ\text{C}$  for cooling cycle).**

Temperature dependence of bulk and grain boundary conductivity of  $\text{Ho}_2\text{Zr}_2\text{O}_7$  pellets sintered using TSS process in both heating and cooling cycles, calculated from the data of impedance measurement are shown in Fig. 7 as Arrhenius plots. The average values of activation energy for bulk and grain boundary conductivity is  $0.99 (\pm 0.009)\text{eV}$  and  $1.40 (\pm 0.004)\text{eV}$  obtained from the combined data of heating and cooling cycles, respectively.

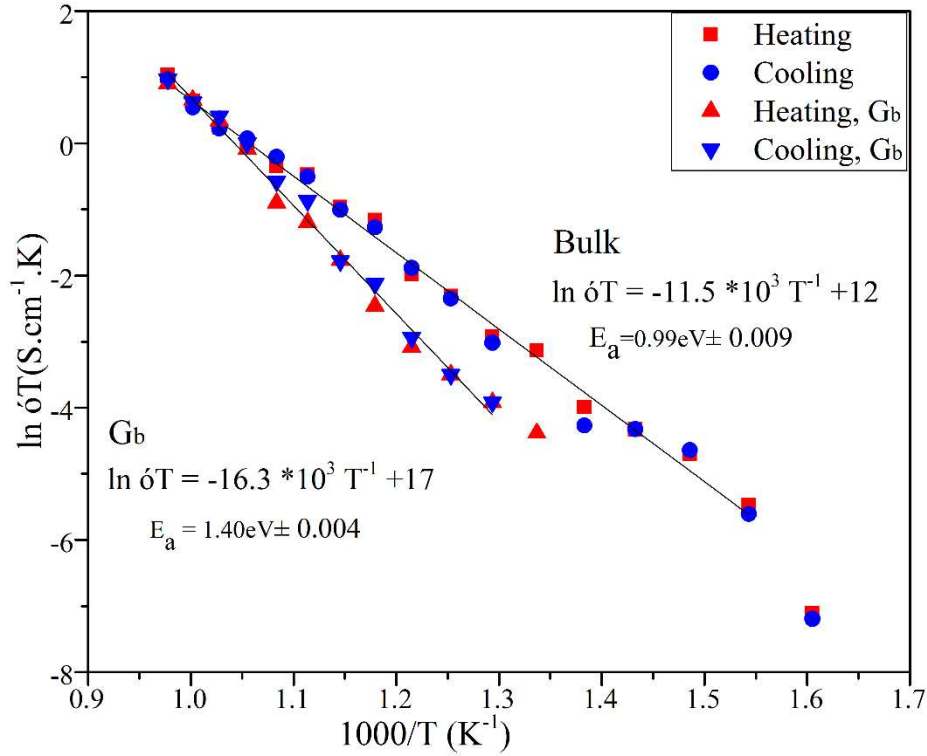


**Fig. 7: Temperature dependence Arrhenius plots of bulk and grain boundary (Gb) conductivity for both heating and cooling cycles of holmium zirconate prepared using TSS process.**

**Table 1: Corresponding activation energies and conductivity values of SSS and TSS processed  $\text{Ho}_2\text{Zr}_2\text{O}_7$**

Sample	Activation Energy (eV)	R <sup>2</sup> value	Conductivity at 550°C S.cm <sup>-1</sup>	Conductivity at 750°C S.cm <sup>-1</sup>
SSS-Bulk	0.99	0.99448	$1.94 \times 10^{-4}$	$1.46 \times 10^{-3}$
SSS-Gb	1.54	0.98864	$4.28 \times 10^{-6}$	$1.66 \times 10^{-4}$
TSS-Bulk	0.99	0.99048	$1.76 \times 10^{-4}$	$2.67 \times 10^{-3}$
TSS-Gb	1.40	0.99433	$5.99 \times 10^{-5}$	$2.50 \times 10^{-3}$

The values of bulk conductivity of  $\text{Ho}_2\text{Zr}_2\text{O}_7$  samples sintered using TSS process  $2.67 \times 10^{-3}$  S.cm<sup>-1</sup> has been found to be greater than  $\text{Ho}_2\text{Zr}_2\text{O}_7$  prepared using SSS process  $1.46 \times 10^{-3}$  S.cm<sup>-1</sup> at 750°C as shown in Table 1. Similar comparison with grain boundary conductivity revealed that the grain boundary conductivity of samples sintered by TSS process is greater than that of SSS process sample by nearly 3 order of magnitude. This is clearly seen in Fig. 8 (a and b), respectively. This clearly suggests that the samples of  $\text{Ho}_2\text{Zr}_2\text{O}_7$  prepared by TSS process has significantly fewer grain boundary defects compared to those processed by SSS process.

Clearly, TSS process is capable of producing nearly perfect sample for further applications in solid state devices. Similar results were reported by Wang et al [22] for CGO.

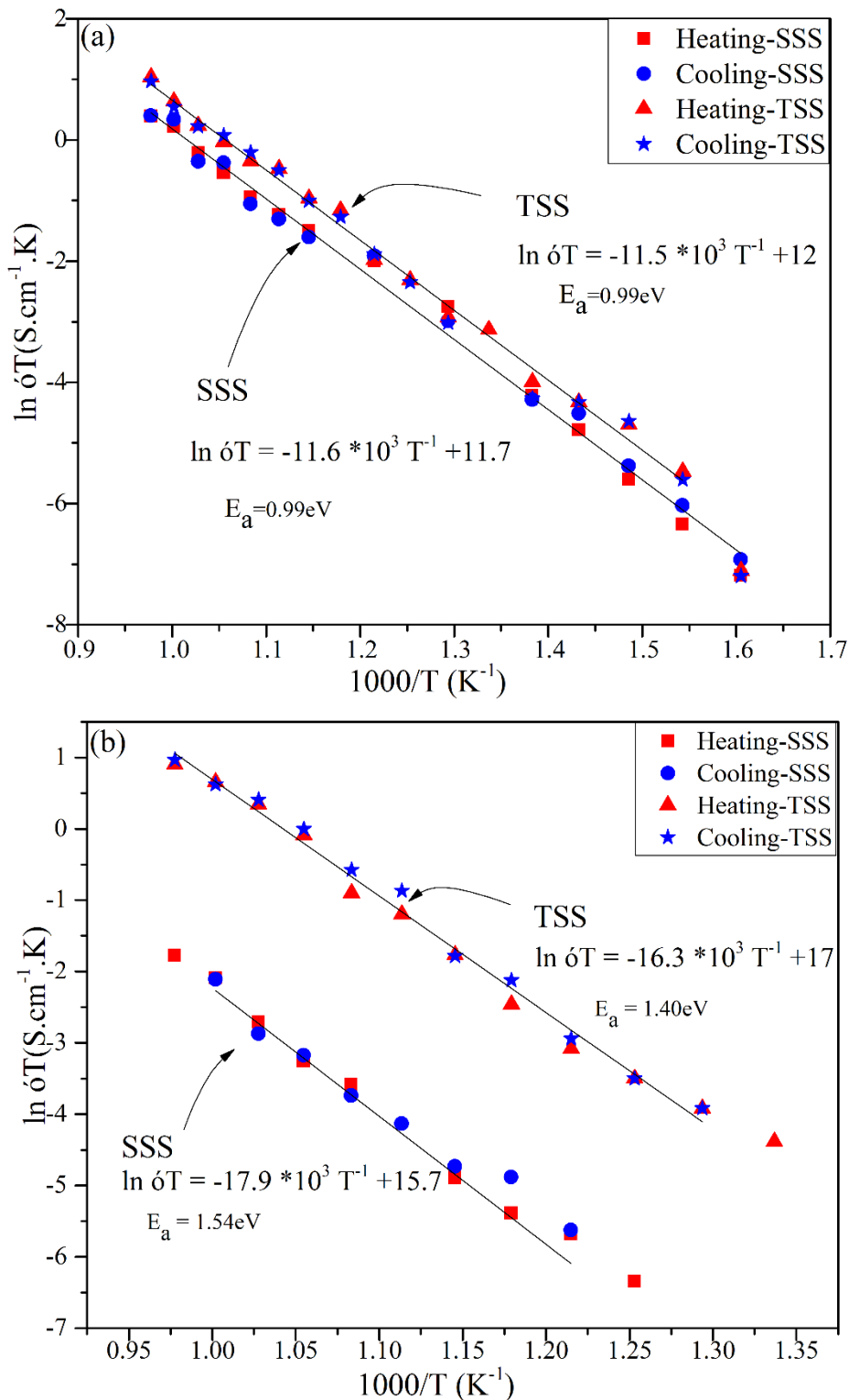


**Fig. 8: Comparison of temperature dependence Arrhenius plots of (a) bulk and (b) grain boundary (Gb) conductivity for both heating and cooling cycles of holmium zirconate prepared using SSS and TSS processes.**

### Conclusions

In this article, the nanopowders of holmium zirconate ( $\text{Ho}_2\text{Zr}_2\text{O}_7$ )<sup>[19]</sup> were compacted into pellets and sintered through conventional (SSS) and unconventional (TSS) sintering routes and impact of processing conditions on microstructure and ionic conductivity were studied. High density  $\text{Ho}_2\text{Zr}_2\text{O}_7$  ceramic was successfully obtained through TSS process with lower grain growth. TSS process has been found to be a better route for processing of ceramics as the relative density of the pellet reaches to 98% at lower temperature (1300°C) with less grain growth as compared to the densification achieved through SSS process at higher temperature (1500°C) with pronounced grain growth 2.2 ( $\pm 0.05$ ) $\mu\text{m}$ . The bulk and grain boundary conductivity of  $\text{Ho}_2\text{Zr}_2\text{O}_7$  processed using SSS and TSS processes were measured over the temperature range of 350°C to 750°C for both heating and cooling cycles using AC impedance spectroscopy in the frequency range of 100 mHz to 100 MHz. The complex impedance plots for SSS and TSS  $\text{Ho}_2\text{Zr}_2\text{O}_7$  exhibit the consistent results for both heating and cooling cycles indicates that solid electrolyte respond reversibly throughout the temperature range of measurement which is an important behaviour of solid electrolyte. The values of bulk ( $2.67 \times 10^{-3} \text{ S.cm}^{-1}$ ) and grain boundary ( $2.50 \times 10^{-3} \text{ S.cm}^{-1}$ ) conductivities of  $\text{Ho}_2\text{Zr}_2\text{O}_7$  pellets prepared using TSS process are higher than that processed using SSS process (Table 1). For SSS  $\text{Ho}_2\text{Zr}_2\text{O}_7$  the activation energy value (0.99eV) of ionic conductivity is comparable with that of SSS CGO<sup>[22]</sup>. The magnitudes of oxide ion conductivity and activation energy for ionic conduction of  $\text{Ho}_2\text{Zr}_2\text{O}_7$  are better than conventional solid electrolytes yttria stabilized zirconia-YSZ (1.01eV) and comparable with gadolinium doped ceria-GDC (0.9 eV)<sup>[25]</sup>. Low sintering temperature, more densification, less grain growth and high ionic conductivity makes the TSS process more preferable route for the processing of solid electrolytes. Holmium zirconate proves to be a promising solid electrolyte by exhibiting excellent and consistent results of ionic conductivity over a wide temperature range with reversible behaviour as solid electrolytes are constantly subject to temperature variation in a practical electrochemical discs such as SOFC or high temperature sensors.

### **Acknowledgement**

The first author would like to thank the Commonwealth Scholarship Commission (CSC), UK for the financial support.

### **Competing financial interests**

The authors declare no competing financial interests.

### **References**

- [1] M. Deepa, R. P. Prabhakar, A. N. Radhakrishnan, K. S. Sibi, P. Koshy, Pyrochlore type semiconducting ceramic oxides in Ca–Ce–Ti–M–O system (M = Nb or Ta)-Structure, microstructure and electrical properties, *Mater. Res. Bull.*, 44 (2009)1481–1488.
- [2] K. S. Sibi, A. N. Radhakrishnan, M. Deepa, R. P. Prabhakar, P. Koshy, Oxide ion conductivity and relaxation in CaREZrNbO<sub>7</sub> (RE = La, Nd, Sm, Gd, and Y) system, *Solid State Ionics*, 180 (2009) 1164–1172.
- [3] J. A. Di'az-Guille'n, A. F. Fuentes, M. R. Di'az-Guille'n, J. M. Almanza, J. Santamari'a and C. J. Leo'n, The effect of homovalent A-site substitutions on the ionic conductivity of pyrochlore-type Gd<sub>2</sub>Zr<sub>2</sub>O<sub>7</sub>, *J. Power Sources*, 186 (2009) 349–352.
- [4] G. T. Knoke, A. Niazi, J. M. Hill and D. C. Johnston, Synthesis, structure, and ferromagnetism of the oxygen defect pyrochlore system Lu<sub>2</sub>V<sub>2</sub>O<sub>7-x</sub> (x=0.40–0.65), *Phys. Rev. B: Condens. Matter Mater. Phys.*, 76 (2007) 054439.
- [5] M. Hirayama, N. Sonoyama, A. Yamada and R. Kanno, Relationship between structural characteristics and photoluminescent properties of (La<sub>1-x</sub>Eu<sub>x</sub>)<sub>2</sub> M<sub>2</sub>O<sub>7</sub> (M=Zr, Hf, Sn) pyrochlores, *J. Lumin.*, 128 (2008) 1819–1825.
- [6] A. Zhang, M. Lu, Z. Yang, G. Zhou and Y. Zhou, Systematic research on RE<sub>2</sub>Zr<sub>2</sub>O<sub>7</sub> (RE = La, Nd, Eu and Y) nanocrystals: Preparation, structure and photoluminescence characterization, *Solid State Sci.*, 10 (2008) 74–81.
- [7] R. C. Ewing, Nuclear waste forms for actinides, *Proc. Natl. Acad. Sci. U. S. A.*, 96 (1999) 3432–3439.
- [8] R. C. Ewing, W. J. Weber and J. Lian, Nuclear waste disposal-pyrochlore (A<sub>2</sub>B<sub>2</sub>O<sub>7</sub>): Nuclear waste form for the immobilization of plutonium and “minor” actinides, *J. Appl. Phys.*, 95 (2004) 5949–5971.
- [9] R. Chow, S. Falabella, G. E. Loomis, F. Rainer, C. J. Stolz, and M. R. Kozlowski, Reactive evaporation of low-defect density hafnia, *Appl. Opt.* 32:28 (1993) 5567-5574.
- [10] R. N. Basu, *Materials for Solid Oxide Fuel Cells, Recent Trends in Fuel Cell Science and Technology*, (2007) 286–331.
- [11] M. A. Subramanian, G. Aravamudan, G. V. S. Rao, *Prog. Solid State Chem.* 1983, 15, 55.
- [12] Shamblin et al., Probing disorder in isometric pyrochlore and related complex oxides, *Nature Materials*. 15 (2016) 507-12
- [13] S. A. Kramer, H. L. Tuller, A novel titanate-based oxygen ion conductor: Gd<sub>2</sub>Ti<sub>2</sub>O<sub>7</sub>, *Solid State Ionics*. 82 (1995) 15.
- [14] M. Stopyra, D. Niemieć, G. Moskal, Synthesis, characterization and thermal diffusivity of holmium and praseodymium zirconates, *Arch. Metall. Mater.* 61 (2016) 1249-1254.

- [15] F.N. Sayed, D. Jain, B.P. Mandal, C.G.S. Pillai, A.K. Tyagi, Tunability of structure from ordered to disordered and its impact on ionic conductivity behavior in the  $\text{Nd}_{2-y}\text{Ho}_y\text{Zr}_2\text{O}_7$  ( $0.0 \leq y \leq 2.0$ ) system, *RSC Adv.* 2 (2012) 8341-8351.
- [16] Z. Wang, G. M. Kale, M. Ghadiri, Synthesis and characterization of  $\text{Ce}_x\text{Gd}_{1-x}\text{O}_{2-d}$  nanopowders employing an alginate mediated ion-exchange process. *Chem. Eng. J.* 198 (2012a) 149–153.
- [17] Z. Wang, G. M. Kale, M. Ghadiri, Novel ion-exchange process for the reparation of metal oxide nanopowders from sodium alginate. *J. Am. Ceram. Soc.* 95 (2012b) 3124–3129.
- [18] Z. Schnepf, S.C. Wimbush, S. Manna, S.R. Hall, Alginate-mediated routes to the selective synthesis of complex metal oxide nanostructures, *Cryst. Eng. Comm.* 12 (2010) 1410–1415, <https://doi.org/10.1039/b923543b>.
- [19] S. Sardar, G.M. Kale, M. Ghadiri, O. Cespedes, 2019. Structural Study of Holmium Zirconate Nanoparticles obtained through Carbon Neutral Sol Gel Process, *Thermochimica Acta.* 676 (2019) 120-129.
- [20] I. W. Chen, X.-H. Wang, Sintering dense nanocrystalline ceramics without final-stage grain growth, *Nature.* 404 (2000). [21] O. Bellon, N. M. Sammes, J. Staniforth, *J Power Sources*, 1998, 75, 116.
- [22] Z. Wang, G. M. Kale, X. Tang, Sintering behavior and ac-conductivity of dense  $\text{Ce}_{0.8}\text{Gd}_{0.2}\text{O}_{1.9}$  solid electrolyte prepared employing single step and two-step sintering process. *Journal of Materials Science.* 49 (8) (2014) 3010-3015.
- [23] S. Guidara, H. Feki, Y. Abid, Impedance, AC Conductivity and Electric Modulus Analysis of L-Leucine L-Leucinium Picrate. *J. Alloys Compd.* 663 (2016) 424–429.
- [24] M. Adamu, G. M. Kale, Novel Sol–Gel Synthesis of  $\text{MgZr}_4\text{P}_6\text{O}_{24}$  Composite Solid Electrolyte and Newer Insight into the  $\text{Mg}^{2+}$ -Ion Conducting Properties Using Impedance Spectroscopy, *J. Phys. Chem. C* 120 (2016) 17909–17915.
- [25] A. S. Mehranjani, D. J. Cumming, D. C. Sinclair, R. H. Rothman, Low-temperature co-sintering for fabrication of zirconia/ceria bi-layer electrolyte via tape casting using a  $\text{Fe}_2\text{O}_3$  sintering aid, *Journal of the European Ceramic Society* 37 (2017) 3981–3993.